Radially localized electron heating in helicon plasmas by X-wave microwave injection

J.S. McKee, ¹ E. E. Scime, ^{1, a)} I. Arnold, ² and S. Loch²

¹⁾ Department of Physics and Astronomy, West Virginia University, Morgantown, WV 26506,

USA

²⁾ Department of Physics, Auburn University, Auburn, AL 36849, USA

(Dated: January 22, 2021)

Here we report on modifications to the electron energy distribution function during X-mode microwave injection in argon and helium helicon plasmas. No electron heating is observed in argon helicon plasmas. Significant electron heating, $\Delta T_e \sim 1$ eV, is observed in helium plasmas. The heating is spatially localized to the upper hybrid resonance layer. Previously absent helium ion emission lines, from states over 50 eV above the helium ion ground state, are observed with the injection of X-mode microwaves.

53

I. INTRODUCTION

10

11

12

14

15

16

17

18

19

20

21

22

23

24

25

26

28

31

32

33

34

37

38

39

40

41

43

49

Control of the electron energy distribution in a plasma is a powerful means of affecting chemical processes within the plasma and the population of excited electronic states. For example, a combination of a resonant driving frequency and catalyst coated electrodes shifts the electron energy distribution out of local thermodynamic equilibrium (LTE) in an atmospheric pressure dielectric barrier discharge and enhances the conversion of carbon dioxide into free carbon and carbon monoxide by as much as 20%. In a helicon plasma source, injection of R-wave microwaves (in both argon and helium plasmas) increases the population of energetic electrons and enhances the number of ions in excited electronic states that are desirable for diagnostic spectroscopy.

It is the targeted enhancement of specific excited electronic states that are used for diagnostic techniques that rely on the absorption or emission of line radiation, e.g., laser induced fluorescence (LIF) and two-photon laserinduced fluorescence (TALIF) diagnostics, ^{3–11} that is the focus of this work. LIF and TALIF employ a laser tuned to a specific atomic or molecular transition to pump electrons to higher energy states. Fluorescent emission arising from the relaxation of the target species is then measured by a photodetector. Standard experimental spectroscopic atomic physics investigation techniques use electron beams to populate specific electronic states. 12 Some groups have demonstrated a similar approach in plasmas, i.e., injection of an electron beam to build up a population of specific excited electronic states that are then targeted for laser based spectroscopy.¹³ A related diagnostic technique is laser collision induced fluorescence (LCIF). 14 LCIF is a variation of the LIF technique. The electrons pumped into the higher energy state by the laser are transferred to nearby atomic or molecular states through collisions. The magnitude of the emission from

In these experiments, X-wave microwave injection into a helicon plasma was performed to increase the total power coupled into the plasma (compared to Rwave injection) and to take advantage of the spatial localization of X-wave absorption to target specific regions of the plasma for later spectroscopic study. Helicon discharges are radio frequency (RF) discharges operated near the lower hybrid frequency. 15 Typical helicon source plasmas densities are $n_e \sim 10^{11} - 10^{14}$ cm⁻³, typical electron temperatures are $T_e \sim 5 - 8$ eV, and typical ion temperatures are $T_i \sim 0.5 \text{ eV}$. These sources operate at a few hundred watts of RF power and typically employ background magnetic fields of a few hundred Gauss for plasma confinement. 16 In recent years, considerable evidence has emerged that plasma production and particle heating (both electron and ion) are dependent on the strong absorption of slow mode waves at the plasma edge. 17–20

At these densities and temperatures, helicon sources are well suited to measurements of the ion velocity distribution function by LIF. During an LIF measurement, the fluorescent emission as a function of the wavelength of a narrow linewidth tunable laser provides a direct measure of the velocity distribution function of an electronic state of the target species. Typically the electronic state selected is metastable to optimize the signal-to-noise ratio of the measurement. The quality of the measured signal depends on the plasma density, the electron temperature, and the background neutral density (through the effects of collisional quenching of the target state by neutrals). While LIF and TALIF techniques have been demonstrated in low temperature plasmas for hydrogen, deuterium, oxygen, nitrogen, xenon, and krypton neutrals^{10,21} and argon and xenon ions,²² no LIF technique has been successfully demonstrated for helium ions. Diagnosing helium flow velocities and ion temperatures in plasmas would contribute significantly to our understanding of plasma dynamos, 23 plasma boundaries, 24 mag-

the collision-populated states provides a measure of the interaction between the laser-excited species and the energetic plasma species capable of driving the collisional transfer.¹⁴

a) Electronic mail: escime@wvu.edu

netic reconnection, ²⁵ and Alfvén waves. ²⁶ The main difficulties are helium's relatively high ionization energy of 24.58 eV and the 40.8 eV energy difference between the lowest level ion metastable state (the 2S state) and the helium ion ground state. These factors result in helium ion metastable populations that are too small to diagnose by LIF for most experiments and applications. ²⁷

96

98

99

101

102

103

104

105

106

107

109

110

112

113

115

116

117

118

119

121

122

123

124

125

126

127

128

129

130

131

132

133

134

135

136

137

138

139

141

142

144

145

147

With the long-term goal of enhancing the helium ion metastable population in mind, modifications to the plasma density and electron energy distribution function (EEDF) due to X-wave absorption in argon and helium helicon plasmas are presented in this work. Our previous R-wave microwave injection experiments demonstrated that microwave heating of helicon plasmas enhanced the high energy tail of the EEDF in argon plasmas while keeping other parameters, like the total particle density, constant. Other helicon source groups have also demonstrated electron heating in argon helicon plasmas with the addition of up to 5.5 kW of R-wave microwaves. In very low pressure argon helicon plasmas, < 0.2 mTorr, Zalach et al. report less than a 1 eV increase in the electron temperature with addition of microwave power until the R-wave power was increased to 5.5 kW. For 5.5 kW of R-wave power, they observed a roughly 1 eV jump in electron temperature.²⁸ However, for our lower power R-wave injection experiments in helium plasmas, there was little change in the population of the excited helium ion states that are needed for TALIF measurements. The concept of using two different energy sources in a plasma to separately control plasma production and species temperature (average energy for non-Maxwellian velocity distributions) is not new. Dual-frequency capacitively coupled plasmas (CCPs)²⁹⁻³² and electron heating in hybrid inductivecapacitive discharges^{33,34} have been explored by other groups with the purpose of enhancing plasma processing rates and etching selectivity by enhancing the high energy portion of the EEDF.

II. EXPERIMENTAL APPARATUS

Measurements were performed in the Compact HElicon for Waves and Instabilities Experiment (CHEWIE) apparatus. A schematic of CHEWIE is shown in Fig. 1. CHEWIE consists of a 60 cm long, 2.5 cm radius Pyrex tube around which is wrapped an m = +1 half-turn helicon antenna. For these measurements, 150 W to 750 W of RF power at 13.56 MHz is coupled to the antenna though a matching network. 16 The reflected RF power, less than 5 W, and the forward power are measured with a BirdTM RF power meter. The tube sits at the center of two 140 turn water-cooled solenoid electromagnets, capable of producing a magnetic field inside the tube of up to 1200 G. The tube and antenna are electromagnetically shielded to protect laboratory electronics from RF interference. The Pyrex tube is connected to a 6-way cross, 8" CF stainless steel expansion cham-

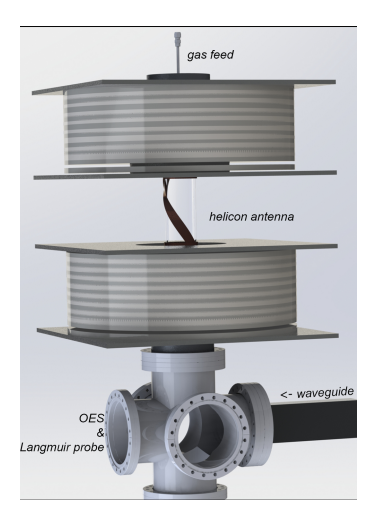


Figure 1. CHEWIE experimental apparatus showing the helicon source, the expansion chamber, and the WR-340 waveguide used for injection of 2.45 GHz microwaves.

ber. The expansion chamber resides in the 'magnetic beach' of the magnetic field profile, which is shown in Fig. 2 for a coil current of 375 A. The chamber is evacuated through a turbo-molecular pumping station from the bottom of the 6-way cross and either argon or helium gas is fed through the gas feed at the top of the system. Unless noted otherwise, all of the argon experiments were performed at an operating pressure of 6.5 mTorr and the helium experiments were performed at an operation pressure of 20 mTorr (the higher helium pressure is required to initiate breakdown with the helicon antenna).

155

159

165

166

168

174

177

Microwaves were injected through a vacuum sealed quartz microwave window on the side of the expansion chamber. The waveguide terminates at the vacuum window, i.e., there is no horn to impedance match the waveguide to the vacuum. The details of the microwave system are shown in Fig. 3. The magnetron and control board are from a Panasonic NN-SN651B household microwave oven, which outputs 1.2 kW of microwave power in 6.4 ms pulses at 120 Hz (70% duty cycle). The microwave power is coupled via a circulator and two-stub tuning network to a WR340 waveguide for TE01 mode transmission at 2.45 GHz. Unlike three stub tuners, a two-stub tuner cannot match all possible impedances, therefore the reflected power (hundreds of Watts) is significant for this system. At 2.45 GHz, the electron cyclotron resonance (ECR) condition, $\omega_{ce} = eB/m_e$, is achieved at 876 G, where e is the electron charge, m_e is the mass of the electron, and B is the magnetic field strength. The reverse power in the circulator is sampled with a crystal diode to adjust reflected power measurements and tune the matching network.

The two primary diagnostics for these experiments were optical emission spectroscopy (OES) and a RF compensated Langmuir probe.³⁵ The light for OES is

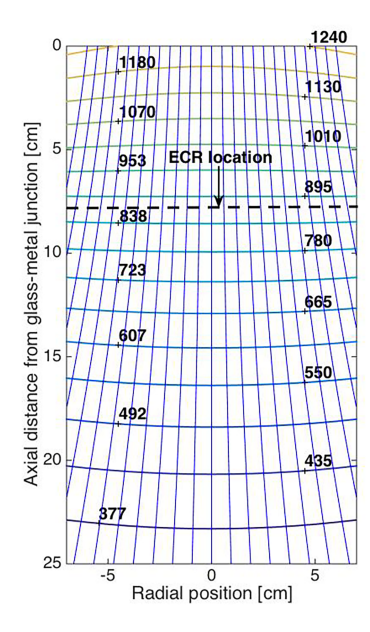


Figure 2. Magnetic field lines (black) and iso-field contours (color) in the expansion chamber for a solenoid current of 375 A. The iso-magnetic field contours are labeled in Gauss. The dashed line shows the location of the electron cyclotron resonance in the system.

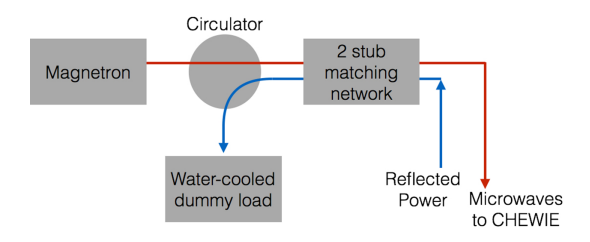


Figure 3. Diagram of the microwave system showing the microwave oven magnetron at 2.45 GHz, the circulator, the matching network, and a water-cooled dummy load.

187

188

189

190

191

192

193

194

195

196

198

199

201

203

collected from the port directly opposite of the microwave injection port. When only microwaves are injected into the chamber, a structure of bright filaments forms in the vacuum chamber in front of the quartz window – a combination of emission from excited ions and neutrals. The collected light is transported to a 1.33 m focal length McPherson model 209 spectrometer (1200 lines/mm grating) by optical fiber and spectra are recorded with a CCD camera. The electron temperature in argon plasmas is determined spectroscopically from the intensity ratio of two closely spaced emission lines (to avoid the need to perform a calibration of wavelength dependent efficiency of the spectrometer). These specific lines were selected because their ratio depends strongly on electron temperature but is relatively insensitive to the plasma density.

The intensity ratio as a function of electron temperature is calculated from a collisional radiative model that employs line strengths obtained from the Atomic

Data and Analysis Structure (ADAS) suite of codes.³⁶ ADAS is an open source set of codes and data sets for modelling ion and atom radiation in plasmas. Shown in Fig. 4 is the line intensity ratio for the 750.593 nm and 751.672 nm lines of neutral argon as a function of electron temperature. Note that the curve shown in Fig. 4 is an overlay of the ratios calculated for plasma densities ranging from 2.5 to $3.5 \times 10^{12} \text{ cm}^{-3}$. Based on the line ratio predicted by the model, a measured line ratio of 1.14 eV corresponds to an electron temperature of 1.14 eV.

207

210

214

216

217

218

223

229

230

232

233

The OES measurements are also used to verify the existence of excited argon and helium ion electronic states. The intensity of emission from different energetic electronic states provides evidence that modifications to the EEDF result in populations of excited and metastable ion states that could be investigated with LIF or TALIF techniques.

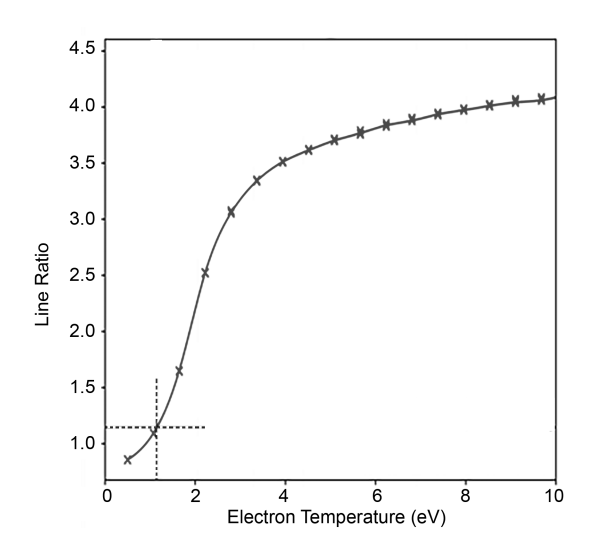


Figure 4. The predicted line intensity ratio for the 750.593 nm and 751.672 nm lines of neutral argon as a function of electron temperature according to a collisional radiative model based on the ADAS line intensity calculations. Line ratio curves are shown for multiple plasma densities ranging from $2.5\text{-}3.5 \times 10^{12} \text{ cm}^{-3}$.

The Langmuir probe was inserted with the tip at 13.5 cm axially in Fig. 2. The tip is a 2 mm diameter 4 mm long graphite rod held by an alumina shaft and press fit into a copper slug shielded by a boron nitride cap. The copper slug is connected to six RF chokes in series with blocking frequencies of 13.56 MHz and its first and second harmonics. For time-averaged measurements of the current-voltage curve of the probe, the probe is biased and the current is read through a Keithley 2400 Sourcemeter. The 0.5 s sweep time of the Keithley prohibits measurements of any time-dependent phenomena during a microwave pulse. Typically, 25 current-voltage traces are averaged together to reduce the effects of random noise in the system.

Since the Langmuir probe radius is much larger than

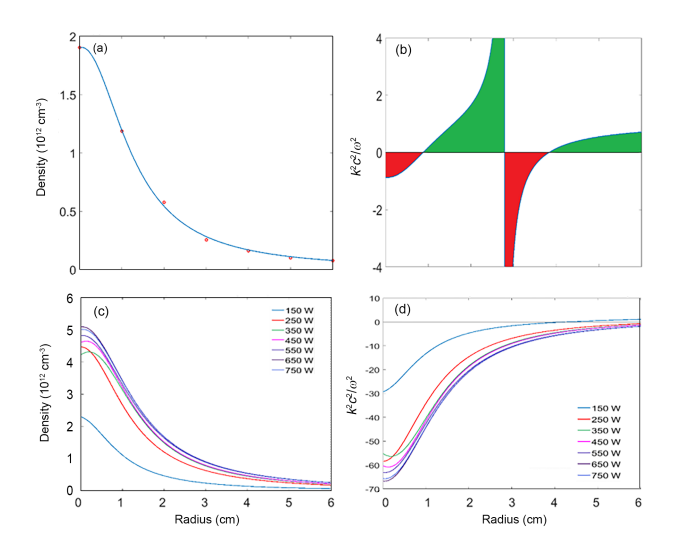


Figure 5. For a source magnetic field of 850 G (a) a typical helium plasma density profile in the expansion chamber. (b) The squared index of refraction $(n^2=k^2c^2/\omega^2)$ in helium plasma. The X-wave propagates in the green region and is evanescent $(n^2<0)$ in the red region. (c) Argon density profiles for different RF powers. (d) The squared index of refraction (n^2) for different RF powers based on the measured density profiles. There is no region of propagation for X-waves $(n^2<0$ everywhere).

the Debye length, $\lambda_D(\sim 10^{-5} \text{ m})$, the ion density is determined from the ion saturation current, I_{sat} , according to

239

240

242

243

245

246

247

248

249

251

252

253

254

256

257

258

259

260

262

$$I_i^{sat} = 0.6n_e e A \sqrt{T_e m_i} \tag{1}$$

where n_e is the plasma density, T_e is the electron temperature, m_i is the ion mass, and A is the collecting area of the probe. The typical Druyvesteyn method of probe trace derivatives is used to obtain the electron temperature and the EEDF.³⁷ For systems where the electron gyro radius, $\rho_e(\sim 10^{-5} \text{ m})$, is smaller than the probe radius and the probe is perpendicular to the magnetic field, Godyak and Demidov showed that the EEDF is given by³⁷

$$f\left(\varepsilon\right) = -\sqrt{e\left(V_{p} - V_{B}\right)} \frac{3m_{e}^{2}}{16\pi^{2}e^{3}\rho_{e}V_{B}} \ln(\pi l 4r_{p}) \frac{dI_{e}}{dV_{B}} \quad (2)$$

where $f(\varepsilon)$ is the EEDF, V_B is the probe bias voltage, V_p is the plasma potential, l is the probe length, r_p is the probe radius, m_e is the electron mass, and I_e is the electron current (total probe current minus the ion contribution). Since I_e increases exponentially with electron temperature in the presence of a non-drifting Maxwellian EEDF, the inverse slope of the natural log of $f(\varepsilon)$ yields the electron temperature. Alternatively, the inverse slope of the natural log of the electron current also yields the electron temperature but that analysis approach does not provide the EEDF. The larger collection area of our large probe makes it

easier to perform the ion saturation current subtraction, however the resultant EEDF may lose accuracy at low energies.³⁷ Because we are interested in the high energy electrons for this work, the 'large' probe (probe radius greater than the electron gyro radius) was used.

The injection waveguide is oriented such that the microwaves propagate perpendicular to the background magnetic field with the wave electric field polarized perpendicular to the background magnetic field, i.e., "extraordinary," X, mode waves. The cold plasma dispersion relation for X mode waves is

$$n^{2} = \frac{k^{2}c^{2}}{\omega^{2}} = \frac{\left(\omega^{2} + \omega\omega_{ce} - \omega_{pe}^{2}\right)\left(\omega^{2} - \omega\omega_{ce} - \omega_{pe}^{2}\right)}{\omega^{2}\left(\omega^{2} - \omega_{ce}^{2} - \omega_{pe}^{2}\right)}$$
(3)

with a resonance at

$$\omega_h = \sqrt{\omega_{ce}^2 + \omega_{pe}^2} \tag{4}$$

and cutoffs at

$$\omega_L = \frac{1}{2} \left[-\omega_{ce} + \left(\omega_{ce}^2 + 4\omega_{pe}^2 \right)^{\frac{1}{2}} \right]$$
 (5)

and

266

270

271 272

275

276

277

281

292

302

$$\omega_R = \frac{1}{2} \left[\omega_{ce} + \left(\omega_{ce}^2 + 4\omega_{pe}^2 \right)^{\frac{1}{2}} \right],$$
(6)

where n is the index of refraction, k is the wavenumber of the wave, c is the speed of light, ω is the wave frequency, $\omega_{ce}=eB/m_e$ is the electron cyclotron frequency for a magnetic field strength B, and the plasma frequency is $\omega_{pe}^2=4\pi n_e e^2/m_e$. The resonant frequency is the upper hybrid frequency, ω_h , and the cutoffs ω_R and ω_L are for left and right circularly polarized waves, respectively. For a microwave frequency of 2.45 GHz and the argon and helium plasma densities used in this study, the electron-electron and electron-ion collision frequencies are orders of magnitude smaller than the microwave frequency. Therefore, collisions have been ignored in the dispersion relation.

The calculated squared index of refraction is shown in Fig. 5b for the measured plasma density profile shown in Fig. 5a and the magnetic field at the axial position of the waveguide. The helicon source tube has a radius of 2.5 cm, so any plasma that appears beyond 2.5 cm arises from cross field transport in the expansion region. Measurements end at $r \sim 6$ cm because bevond that the density is too small for reliable Langmuir probe measurements. There are two clear regions of negative squared index of refraction (evanescent propagation) and a resonance around a radial location of 2.5 cm. Therefore, for X-mode microwaves to reach the resonance layer in a plasma with a peak density of $2 \times 10^{12} \text{ cm}^{-3}$, they would have to tunnel through a narrow evanescent region. The measured plasma density profiles for argon plasmas in CHEWIE as function of RF power are shown in Fig. 5c. In all cases, the

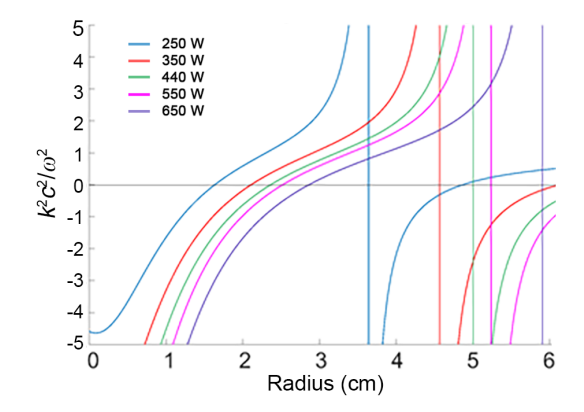


Figure 6. For a source magnetic field of 850 G, the calculated squared index of refraction $(n^2=k^2c^2/\omega^2)$ for helium plasma as a function of helicon source RF power as a function of radial location. There are clear regions of X-wave propagation $(n^2>0)$ and an upper hybrid resonance for all RF powers.

simple cold plasma dispersion relation (Fig. 5d) predicts that X-mode waves will never reach a resonant layer because the plasma is "overdense" for the given microwave frequency and local magnetic field strength. For argon plasmas, we should not expect to see significant electron heating for X-wave injection. Note that in our previous studies in which microwaves were injected along the magnetic field (as R-waves), significant, but not large, electron heating at the cyclotron resonance was observed for argon plasmas and very weak heating was observed in helium plasmas.² Since electron heating in helium plasmas was desired, the experiment was reconfigured to permit X-mode injection.

The calculated squared index of refraction for helium plasmas in CHEWIE plasmas is shown in Fig. 6 for different helicon source RF powers. Because of the lower overall density of helium helicon plasmas, a resonance appears in the plasma at the upper frequency and if the X-mode microwaves are able to tunnel through the thin evanescent region, some microwave energy should be deposited in the plasma. The predicted location for the resonance moves radially outward with increasing RF power.

III. RESULTS

312

313

314

315

317

318

319

320

321

322

323

324

325

326

327

328

329

330

331

332

333

334

335

336

337

338

339

340

341

342

344

Langmuir probe measurements of the electron temperature radial profiles are shown in Fig. 7 for three different RF powers. Measurements with and without the microwave system turned on are shown. Also shown are EEDF measurements for all three RF powers (250, 450, and 650 Watts) and both microwave powers (on and off) for two different radial locations (1 cm and 5 cm). The electron temperature profile peaks at 4 eV on axis and drops rapidly to 1 eV by $r=3.5~\rm cm$. Outside of 3.5 cm, the electron temperature is constant at

roughly 1 eV. Near the axis $(r=1~{\rm cm})$, the log of the EEDF is linear from 5 to 20 eV, indicative of a single Maxwellian velocity distribution. Further out $(r=5~{\rm cm})$, the EEDF remains Maxwellian but reaches the noise floor in the measurement by 9 eV – consistent with a much colder electron population. The key feature in the all the measurements is the clear lack of any electron heating or enhancement of the EEDF at any energy when the microwaves are injected into the argon plasma

348

354

355

356

364

365

370

377

389

390

391

OES measurements of argon neutral and argon neutral emission paint a similar picture of the effects of microwave injection. Shown in Fig. 8 is the emission spectrum around 667 nm for an RF power of 250 Watts. The neutral lines show a clear increase in intensity with the microwave injection, while the ion lines are unchanged with the injection of microwaves. The OES measurements are line integrated and therefore contributions from the edge of the plasma, where neutrals dominate, are added to the contributions from the ions, which are largest near the center of the plasma. It is likely that the increase in neutral line emission reflects deposition of microwave energy at the periphery of the plasma – consistent with the lack of observed electron heating for $r<6\ {\rm cm}.$

Corroborating the probe measurements which show no change in electron temperature with microwave injection are electron temperatures determined from the argon neutral line ratio per Fig. 4. Shown in Fig. 9a are measurements of the electron temperature from the ratio of the line-of-sight integrated intensities of the neutral argon 750.593 nm and 751.672 nm lines. As expected, the neutral line intensity ratio method yields electron temperatures consistent with the Langmuir probe derived electron temperatures in the outer region of the plasma for the same RF power (roughly 1.5 eV). For most RF powers, there is no change in the electron temperature with and without the microwaves. The line ratio method is extremely sensitive to highest energy portion of the EEDF and there might be a statistically significant increase in the electron temperature for the lowest RF power case shown in Fig. 9a. This is consistent with Fig. 8, which showed some increase in neural argon line emission at low RF powers – most likely limited to the periphery of the plasma.

The electron heating results are very different for helium plasmas. Shown in Fig. 10 are Langmuir probe measurements of the electron temperature radial profiles in helium plasmas for three different RF powers. Measurements with and without the microwave system turned on are shown. Also shown are EEDF measurements for all three RF powers (250, 450, and 650 Watts) and both microwave powers (on and off) for two different radial locations (1 cm and 5 cm). For all three RF powers, there is a nearly 1 eV increase in the electron temperature around $r=2.5~\rm cm$.

The EEDFS at both locations shown (r = 1 cm) and r = 5 cm are clearly not describable with a sin-

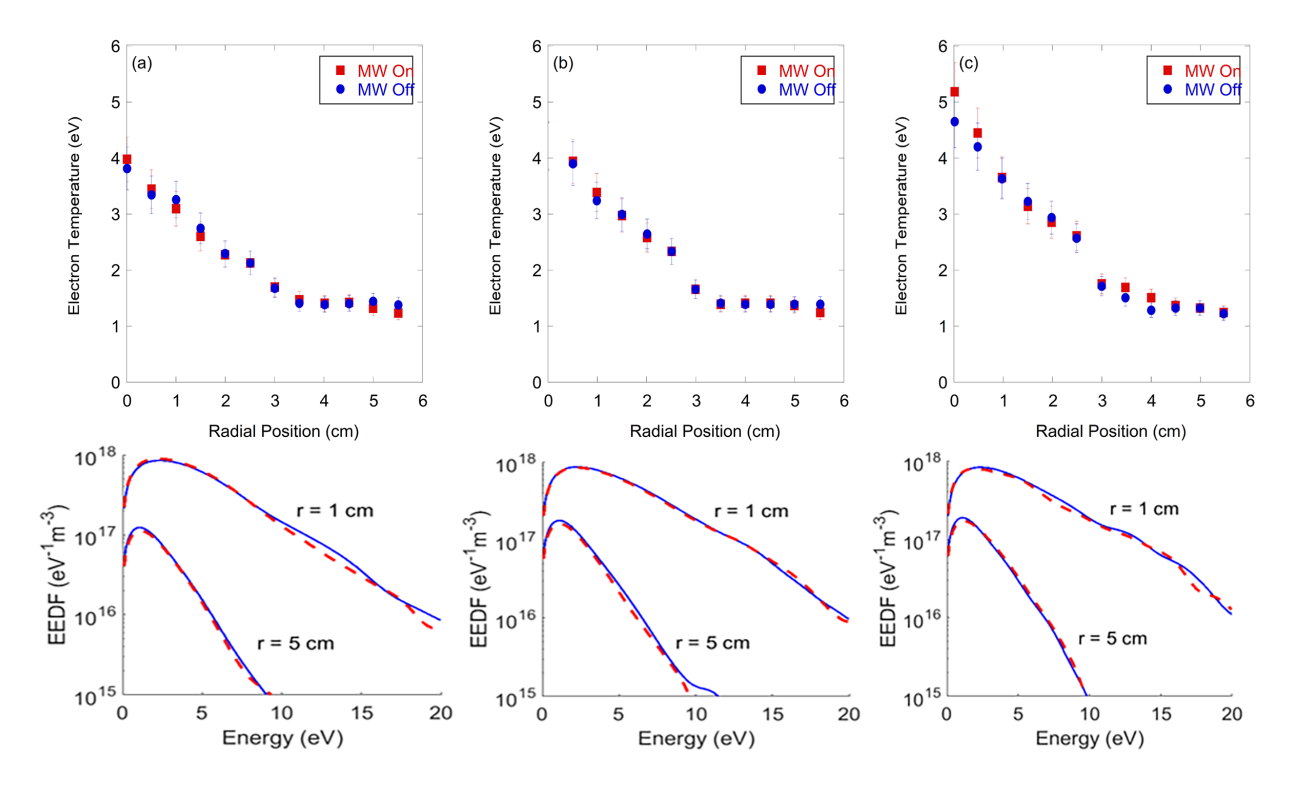


Figure 7. Argon electron temperature (from Langmuir probe measurements) versus radial location for three different Rf powers (a) 250 W, (b) 450 W, and (c) 650 W with (red squares) and without (blue circles) microwaves. Below each radial profile, the electron energy distribution function (EEDF) obtained from a Druyvesteyn analysis for the same RF powers with (red dashed lines) and without (blue solid lines) microwaves is shown for two different radial positions.

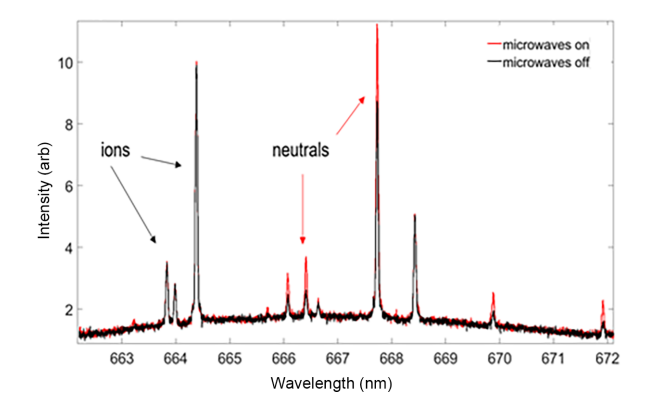


Figure 8. The argon emission spectrum for an RF power of $250~\mathrm{W}$ with (red) and without (black) microwave injection. The spectrum includes emission from both neutral argon and argon ions.

gle Maxwellian energy distribution. Enhancement of the high energy tail of the EEDF is typical in helicon sources. ²⁰ As the RF power increases, a discontinuity in the EEDF shifts from roughly 12 eV at an RF power of 250 W to roughly 7 eV for an RF power of 650 W. The portion of the EEDF above this breakpoint energy decreases in amplitude with the introduction of X-wave microwaves. Further out from the CHEWIE axis $(r=5\,\mathrm{cm})$ the changes in the EEDF are dramatic. For nearly

all energies, there is significant increase in the EEDF amplitude and the slope of the EEDF decreases (electron temperature increases). The EEDF at $r=3\,\mathrm{cm}$ for an RF power of 650 W is shown in Fig. 11 with and without microwaves. The electron temperature in this helium plasma jumps nearly 1.5 eV with the addition of the X-wave microwaves. The amplitude of the EEDF for all energies above 20 eV increases significantly when the microwaves are injected. By 35 eV, the increase in EEDF amplitude is nearly an order of magnitude. The X-mode microwaves clearly enhance the energetic electron population at the location of the upper hybrid resonance.

OES measurements of helium ion emission paint a similar picture of the effects of microwave injection. Shown in Fig. 12 is the emission spectrum around 468.6 nm and 656.0 nm for an RF power of 250 Watts, a neutral pressure of 20 mTorr, and without microwave injection. Also shown is the emission spectrum for the same RF power and for two different operating pressures (20 mTorr and 7 mTorr) with injection of microwaves. The 656.0 nm transition arises from decay of the n=6 level of the helium ion to the n=4 level whereas the 468.6 nm line arises from decay of the n=4 level to the n=3 level. For both transitions the OES measurements show no evidence of emission without microwave injection and clear evidence of emission with microwave injection. The increase in emission is much greater for

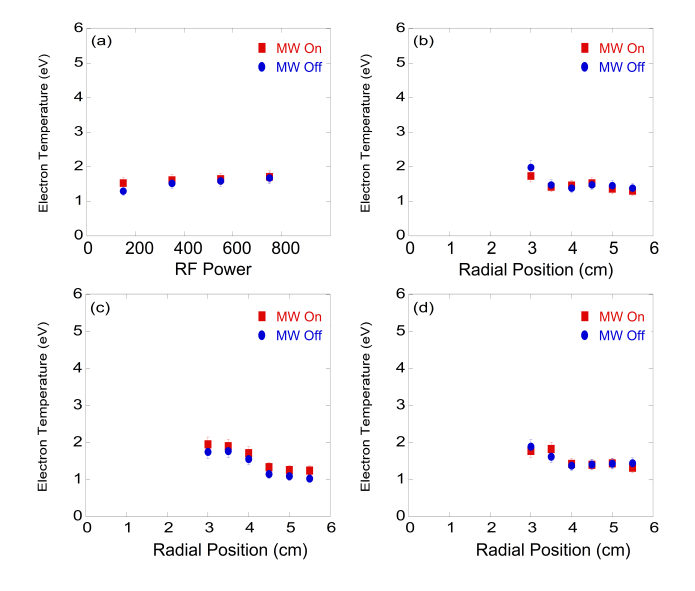


Figure 9. (a) Argon electron temperature determined from neutral line emission ratio for four different Rf powers with (red) and without (red) microwaves. (b) The Langmuir probe measured electron temperature for an RF power of 350 Watts as a function of radial location. (c) The Langmuir probe measured electron temperature for an RF power of 550 Watts as a function of radial location. (d) The Langmuir probe measured electron temperature for an RF power of 750 Watts as a function of radial location. The emission based electron temperatures are generally consistent with the probe measurements around $r \sim 3.5~{\rm cm}$

the 7 mTorr case compared to the 20 mTorr case. The observed increase in helium ion emission for these X-wave injection experiments was much larger than what was observed in the earlier R-wave injection studies.² We note that the strong line at 656.3 nm is a hydrogen line due to residual water in the system.

The Langmuir probe and OES measurements both confirm coupling of microwave power into the electrons and the Langmuir probe measurements localize the heating to roughly r=2.5 cm, exactly where the upper hybrid resonance is expected for these plasma conditions.

453 IV. DISCUSSION

441

442

443

445

446

447

448

449

450

451

452

454

455

457

458

459

460

461

463

These measurements demonstrated spatially localized heating of electrons at the upper hybrid resonance in helium helicon plasmas through the injection of X-mode microwaves. No heating was observed in argon helicon plasmas, as expected given the lack of an upper hybrid resonance in argon plasmas for a microwave frequency of 2.45 GHz. Because the long-term objective of these experiments is to enhance the fraction of helium ions in the very energetic (40.8 eV above the ground state) metastable 2S state, it is important to consider the impact of the increased electron temperature on the

population of 2S state. As shown in Fig. 12, the gain in electron energy due to the microwave injection is clearly sufficient to drive helium ions into the n=6 state, 52.9 eV above the ground state. Shown in Fig. 13 is the relative population, relative to the ground state density, of the 2S metastable state as a function of electron temperature for four different plasma densities. The curves shown in Fig. 13 are again from on a collisional radiative model of helium that uses the rate coefficients for helium neutral and helium ion transitions from the ADAS suite of codes. Based on the model shown in Fig. 13, the observed 3.5 to 5.0 eV change in electron temperature in the 650 W helium plasma at r=3cm should result in at least a twenty fold increase in the helium 2S metastable ion population. With such a change in excited state population, it may then be possible to deploy LIF and TALIF techniques in helium helicon plasmas for direct measurements of the helium ion velocity distribution function. Note that is is possible that microwave injection has the potential to alter the original ion velocity distribution through collisional heating of the ions by hotter electrons, an effect that should be considered if this technique proves successful in creating the appropriate metastable population for TALIF.

V. ACKNOWLEDGEMENTS

467

470

473

474

476

478

479

491

493

496

497

500

501

502

503

504

505

506

507

508

509

510

511

512

513

515

This work is supported by US National Science Foundation (NSF) grants number PHY-1902111 and OIA-1655280. We thank Gerling Applied Engineering for 2.45 GHz microwave source guidance.

5 DATA AVAILABILITY

The data that support the findings of this study are available from the corresponding author upon reasonable request.

REFERENCES

¹M. A. Lindon and E. E. Scime, "Co2 dissociation using the versatile atmospheric dielectric barrier discharge experiment (vader)," Frontiers in Phys. **2**, 55 (2014).

²M. U. Siddiqui, J. S. McKee, J. McIlvain, Z. D. Short, D. B. Elliott, G. Lusk, and E. E. Scime, "Electron heating and density production in microwave-assisted helicon plasmas," Plasma Sources Sci. & Technol. 24 (2015), 10.1088/0963-0252/24/3/034016.

³D. N. Hill, S. Fornaca, and M. G. Wickham, "Single frequency scanning laser as a plasma diagnostic," Rev. Sci. Instrum. 54, 309–314 (1983), https://doi.org/10.1063/1.1137389.

⁴G. D. Severn, D. A. Edrich, and R. McWilliams, "Argon ion laser-induced fluorescence with diode lasers," Rev. Sci. Instrum.
69, 10–15 (1998), https://doi.org/10.1063/1.1148472.

⁵A. M. Keesee, E. E. Scime, and R. F. Boivin, "Laser-induced fluorescence measurements of three plasma species with a tun-

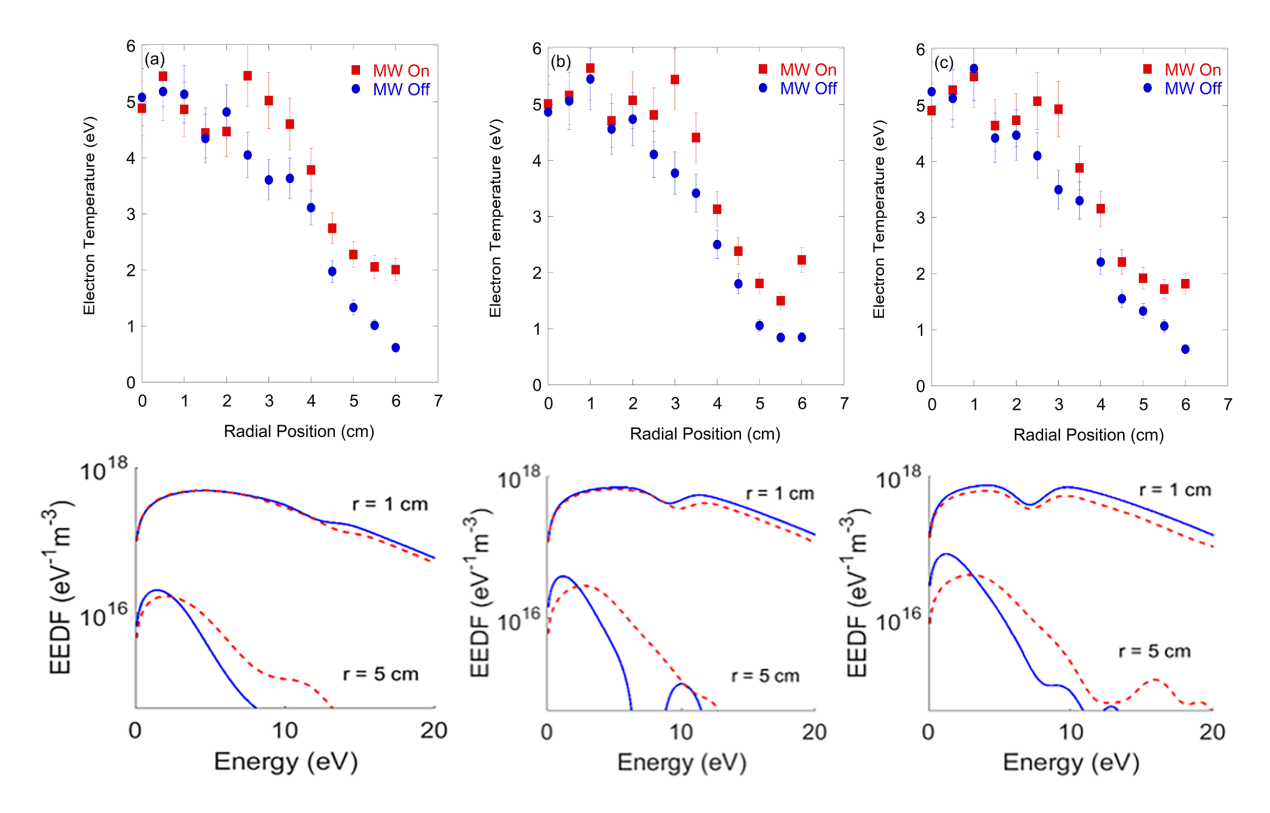


Figure 10. Helium electron temperature (from Langmuir probe measurements) versus radial location for three different RF powers (a) 250 W, (b) 450 W, and (c) 650 W with ith (red squares) and without (blue circles) microwaves. Below each radial profile, the electron energy distribution function (EEDF) obtained from a Druyvesteyn analysis for the same RF powers with (red dashed lines) and without (blue solid lines) microwaves is shown for two different radial positions. The electron heating is well outside of the 10% error bars shown.

523

524

525

526

527

528

529

530

531

532

533

534

535

536

537

538

539

540

541

542

543

544

545

546

547

548

549

550

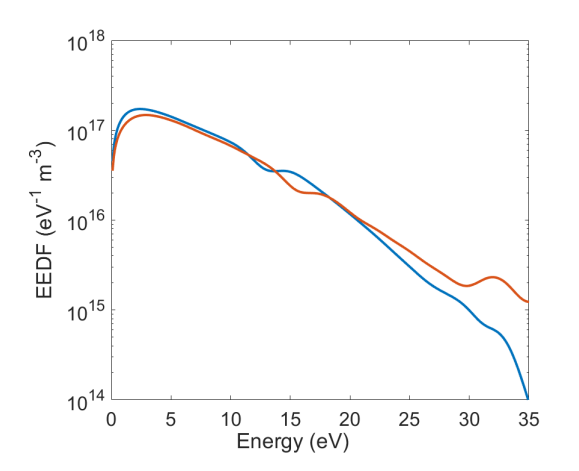


Figure 11. The EEDF at r=3 cm for an RF power of 650 W with (red) and without (blue) microwave injection. The high energy portion of the EEDF exhibits significant enhancement with the addition of the microwaves.

able diode laser," Rev. Sci. Instrum. **75**, 4091–4093 (2004), https://doi.org/10.1063/1.1787166.

516

517

518

519

520

⁶R. F. Boivin and E. E. Scime, "Control of nitrogen species in helicon plasmas," Plasma Sources Sci. & Technol. 14, 283–292 (2005). ⁷E. Scime, C. Biloiu, C. Compton, F. Doss, D. Venture, J. Heard, E. Choueiri, and R. Spektor, "Laser induced fluorescence in a pulsed argon plasma," Rev. Sci. Instrum. **76**, 026107 (2005), https://doi.org/10.1063/1.1848491.

⁸ A. M. Keesee and E. E. Scime, "Neutral density profiles in argon helicon plasmas," Plasma Sources Sci. & Technol. 16, 742–749 (2007).

⁹I. A. Biloiu and E. E. Scime, "Temporal evolution of double layers in pulsed helicon plasmas," App. Phys. Lett. **95**, 051504 (2009), https://doi.org/10.1063/1.3204014.

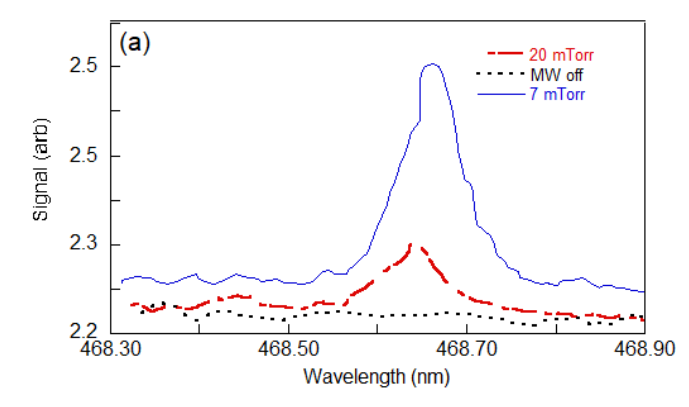
¹⁰R. M. Magee, M. E. Galante, D. McCarren, E. E. Scime, R. L. Boivin, N. H. Brooks, R. J. Groebner, D. N. Hill, and G. D. Porter, "A two photon absorption laser induced fluorescence diagnostic for fusion plasmas," Rev. Sci. Instrum. 83, 10D701 (2012), https://doi.org/10.1063/1.4728092.

¹¹M. E. Galante, R. M. Magee, and E. E. Scime, "Two photon absorption laser induced fluorescence measurements of neutral density in a helicon plasma," Phys. Plasmas 21, 055704 (2014), https://doi.org/10.1063/1.4873900.

¹²R. Lockwood, L. Anderson, and C. Lin, "A method for measuring cross-sections for electron-impact excitation out of metastable levels of atoms," Zeitschrift Fur Physik D-Atoms Molecules and Clusters 24, 155–160 (1992).

¹³G. Langhans, W. Schade, and V. Helbig, "Lifetime measurements of the Kr-III 5p(5)p(3) level using time-resolved laser-induced fluorescence spectroscopy," Phys. Lett. A 183, 205–208 (1993).

¹⁴E. V. Barnat and B. R. Weatherford, "2D laser-collision induced fluorescence in low-pressure argon discharges," Plasma Sources Sci. & Technol. **24** (2015), 10.1088/0963-0252/24/5/055024.



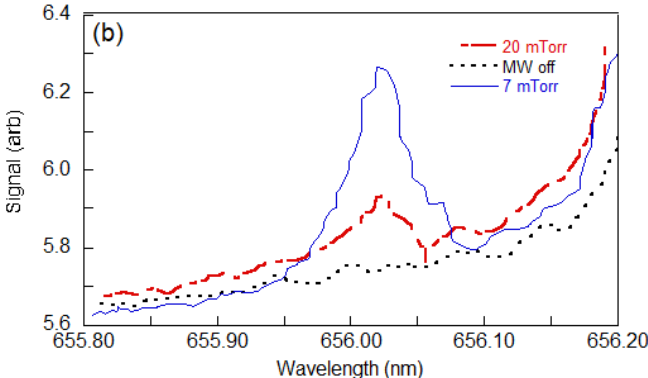


Figure 12. (a) Emission around the 468 nm He II transition for two different pressures (20 mTorr and 7 mTorr) with microwaves and without (black dotted line). (b) Emission around the 656 nm He II transition for two different pressures (20 mTorr and 7 mTorr) with microwaves and without (black dotted line). The magnetic field strength was 850 G and the RF power was 250 kW. The operating pressure was 20 mTorr for the no microwave case.

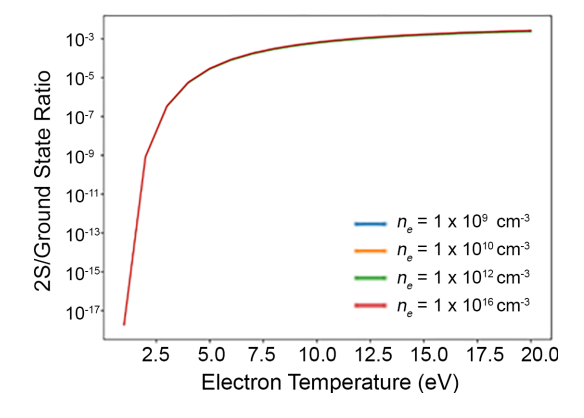


Figure 13. The predicted population in the 2S state of He II relative to the ground state as a function of electron temperature for four different electron densities. The predicted ratio is insensitive to density over seven orders of magnitude.

¹⁵R. W. Boswell, "Very efficient plasma generation by whistler waves near the lower hybrid frequency," Plasma Phys. and Controlled Fusion 26, 1147–1162 (1984).

¹⁶M. Balkey, R. Boivin, J. Kline, and E. Scime, "Ion heating and density production in helicon sources near the lower hybrid frequency," Plasma Sources Sci. & Technol. 10, 284–294 (2001).

¹⁷R. T. S. Chen and N. Hershkowitz, "Multiple electron beams generated by a helicon plasma discharge," Phys. Rev. Lett. 80, 4677–4680 (1998).

¹⁸J. Kline, E. Scime, R. Boivin, A. Keesee, X. Sun, and V. Mikhailenko, "rf absorption and ion heating in helicon sources," Phys. Rev. Lett. 88 (2002), 10.1103/Phys-RevLett.88.195002.

¹⁹E. M. Aguirre, E. E. Scime, D. S. Thompson, and T. N. Good, "Spatial structure of ion beams in an expanding plasma," Phys. Plasmas 24 (2017), 10.1063/1.5003722.

²⁰E. M. Aguirre, R. Bodin, N. Yin, T. N. Good, and E. E. Scime, "Evidence for electron energization accompanying spontaneous formation of ion acceleration regions in expanding plasmas," Phys. Plasmas 27 (2020), 10.1063/5.0025523.

²¹K. Niemi, V. S. von der Gathen, and H. F. Döbele, "Absolute calibration of atomic density measurements by laser-induced fluorescence spectroscopy with two-photon excitation," Journal of Phys. D: App. Phys. 34, 2330-2335 (2001).

²²D. Lee, N. Hershkowitz, and G. D. Severn, "Measurements of ar+ and xe+ velocities near the sheath boundary of ar-xe plasma using two diode lasers," App. Phys. Lett. **91**, 041505 (2007), https://doi.org/10.1063/1.2760149.

²³E. J. Spence, K. Reuter, and C. B. Forest, "A spherical dynamo experiment," The AstroPhys. Journal **700**, 470–478 (2009).

²⁴I. A. Biloiu and E. E. Scime, "Ion acceleration in ar-xe and ar-he plasmas. ii. ion velocity distribution functions," Phys. Plasmas 17, 113509 (2010), https://doi.org/10.1063/1.3505823.

²⁵I. Furno, T. Intrator, E. Torbert, C. Carey, M. D. Cash, J. K. Campbell, W. J. Fienup, C. A. Werley, G. A. Wurden, and G. Fiksel, "Reconnection scaling experiment: A new device for three-dimensional magnetic reconnection studies," Rev. Sci. Instrum. **74**, 2324–2331 (2003), https://doi.org/10.1063/1.1544051.

²⁶S. Houshmandyar and E. E. Scime, "Ducted kinetic alfvén waves in plasma with steep density gradients," Phys. Plasmas 18, 112111 (2011), https://doi.org/10.1063/1.3662113.

²⁷J. Winter, J. S. Sousa, N. Sadeghi, A. Schmidt-Bleker, S. Reuter, and V. Puech, "The spatio-temporal distribution of he (23s1) metastable atoms in a MHz-driven helium plasma jet is influenced by the oxygen/nitrogen ratio of the surrounding atmosphere," Plasma Sources Sci. & Technol. 24, 025015 (2015).

²⁸J. Zalach, O. Grulke, and T. Klinger, "Ecr heating in a helicon device," AIP Conference Proceedings 812, 219–222 (2006), https://aip.scitation.org/doi/pdf/10.1063/1.2168827.

²⁹T. Gans, J. Schulze, D. O'Connell, U. Czarnetzki, R. Faulkner, A. R. Ellingboe, and M. M. Turner, "Frequency coupling in dual frequency capacitively coupled radiofrequency plasmas," App. Phys. Lett. 89, 261502 (2006), https://doi.org/10.1063/1.2425044.

³⁰ J. Schulze, E. Schüngel, U. Czarnetzki, and Z. Donkó, "Optimization of the electrical asymmetry effect in dual-frequency capacitively coupled radio frequency discharges: Experiment, simulation, and model," Journal of App. Phys. **106**, 063307 (2009), https://doi.org/10.1063/1.3223310.

³¹È. Schüngel, J. Schulze, Z. Donkó, and U. Czarnetzki, "Power absorption in electrically asymmetric dual frequency capacitive radio frequency discharges," Phys. Plasmas 18, 013503 (2011), https://doi.org/10.1063/1.3535542.

³²B. B. Sahu and J. G. Han, "Electron heating mode transition induced by mixing radio frequency and ultrahigh frequency dual frequency powers in capacitive discharges," Physics of Plasmas 23, 053514 (2016), https://doi.org/10.1063/1.4952629. ³³M.-H. Lee, H.-C. Lee, and C.-W. Chung, "Observation of collisionless heating of low energy electrons in low pressure inductively coupled argon plasmas," App. Phys. Lett. **93**, 231503 (2008), https://doi.org/10.1063/1.3042264.

- ³⁴H.-C. Lee and C.-W. Chung, "Control of electron energy distribution by adding a pulse inductive field in capacitive discharge," Plasma Sources Sci. & Technol. 23, 062002 (2014).
- ³⁵P. A. Keiter, Experimental Investigation of Ion Temperature
 Anisotropy Driven Instabilities in a High Beta Plasma, Ph.D.
 thesis, West Virginia University (1999).
- ³⁶ A. D. W. N. R. B. H. P. Summers, M. G. O'Mullane and S. D.
 Loch, "Adas: Atomic data, modelling and analysis for fusion,"
- AIP Conf. Proc. ATOMIC AND MOLECULAR DATA AND THEIR APPLICATIONS: 5th International C onference on Atomic and Molecular Data and Their Applications (ICAM-DATA). 901, 239–248 (2007).

- ³⁷V. A. Godyak and V. I. Demidov, "Probe measurements of electron-energy distributions in plasmas: what can we measure and how can we achieve reliable results?" Journal of Phys. D: App. Phys. 44, 233001 (2011).
- ³⁸Hershkowitz N, How Langmuir probes work in Plasma Diagnostics 1 (Academic, 1989) p. 83–113.